Journal of Materials Research and Technology 33 (2024) 5142–5148

Contents lists available at ScienceDirect

Journal of Materials Research and Technology

journal homepage: www.elsevier.com/locate/jmrt

Constitutive modeling of the slip-twinning transition in martensitic transformations

Sheron Stephany Tavares, Marc André Meyers *

Program of Materials Science and Engineering, University of California San Diego, La Jolla, CA, 92093, USA

ARTICLE INFO

Handling editor: L Murr

Keywords:
Martensite
Slip
Twinning

ABSTRACT

Martensite is the result of a diffusionless displacive phase transition. In Fe-based alloys it transforms the FCC to the BCC, BCT, or HCP structures and occurs at high strain rates. It has two typical morphologies, known as lath and plate. A quantitative constitutive description of the slip-twinning transition in the martensitic transformation is presented. It is based on the temperature and strain-rate sensitivities of slip, which are much higher than those for twinning. Thus, twinning becomes a favored deformation mechanism at low temperatures and high strain rates. The Hall-Petch coefficient, for the inclusion of grain size effects, is two times larger for twinning than slip. Constitutive relationships for slip and twinning are presented and applied to the martensitic transformation in steels; the lath-to-plate morphology change observed with increasing carbon content is successfully predicted as a function of grain size by calculations incorporating the two modes of deformation. A simple calculation of the strain rates during martensitic transformation is also provided. This methodology is applied to the Fe–C system and can be extended to the Fe–Ni–C system and to thermoelastic martensites, where twinning is favored over slip to enhance reversibility.

1. Introduction

Ulrich Frederick Kocks contributed to the fabric of materials science in a significant way, His career and major impact in the field are described in detail by Ashby [1], in this Special Issue. His first important contribution was a statistical theory of the flow stress and work hardening [2]. He dedicated great effort to the effect of solid solutions on hardening and studied the manner by which foreign atoms interact with crystal defects. Later, he considered more complex slip mechanisms and, specifically, strain aging [3]. His most famous contribution, addressing the thermodynamics and kinetics of slip, was co-authored by Michael Ashby and Ali Argon [4]. Later, at Los Alamos National Laboratory, he developed, with Paul Follansbee, a constitutive description of work hardening, applied to copper, based on the use of a mechanical threshold stress as an internal state variable [5]. This became the basis for the Mechanical Threshold Stress (MTS) model of temperature and strain-rate-dependent work hardening, also referred to as the Kocks-Mecking model. Our group had the occasion to apply the Kocks model incorporating dislocation generation and annihilation to tantalum, with excellent results [6].

It is well known that slip and twinning are competing deformation mechanisms. The competition between these mechanisms has been modeled by Meyers et al. [7], among others. Fig. 1 shows, in schematic fashion, how the temperature and strain rate dependence of these two mechanisms determines the resulting microstructure. The temperature and strain rate dependence of slip are much higher than those for twinning. The latter is, in a simplified manner, assumed to be constant. Thus, a lower temperature and higher strain rate favor twinning. Such a situation also takes place in martensitic transformation. This plot, although qualitative, provides deep insight into the mechanical response of metals and alloys, which can deform by slip, twinning, or martensitic transformations.

Thomas [8,9] showed that the transition from one mechanism to the other profoundly affects the mechanical properties of martensitic steels. Martensitic transformations are displacive, virtually diffusionless transformations with the thermodynamics and kinetics governed by the transformation strains.

Continuing the work of Thomas, Schneider et al. [9] applied constitutive equations for slip and twinning and obtained successfully the prediction of the slip-twinning transition. This is the foundation for the contribution presented here.

Wang and Sehitoglu [10] performed a theoretical energetic, rather

* Corresponding author.
E-mail address: mameyers@ucsd.edu (M.A. Meyers).

https://doi.org/10.1016/j.jmrt.2024.10.151
Received 26 July 2024; Received in revised form 1 October 2024; Accepted 15 October 2024
Available online 17 October 2024

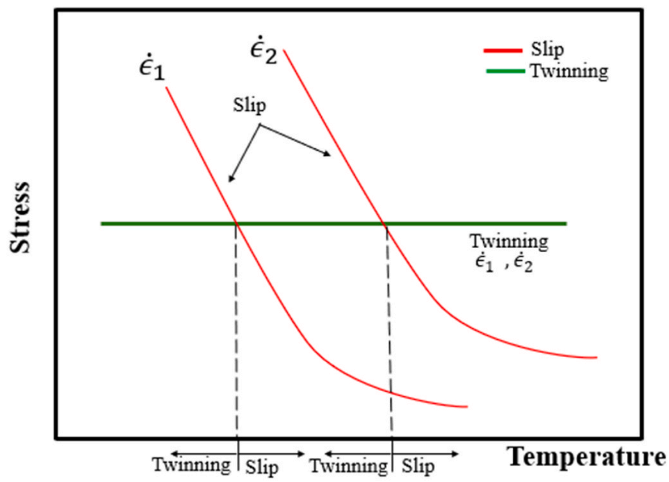

Fig. 1. Variation of the stress for slip and twinning as a function of temperature at two strain rates. The operating deformation mechanism is assumed to be the one that requires less stress. The slip to twinning transition is dependent on strain rate. The composition variations are expected to affect the slip-twin cross-over, as suggested by the arrows.

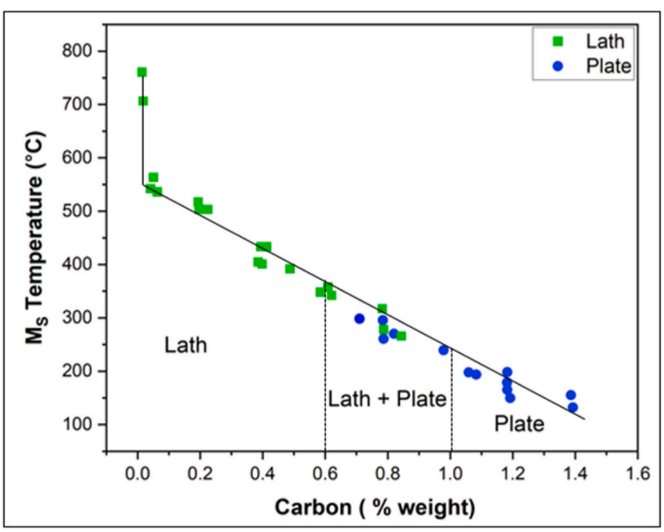

Fig. 2. Variation of *Ms* temperature with carbon content, notice the transition from lath (slipped) to plate (twinned) morphology (Adapted from Marder and Kraus [18]).

than stress-based analysis and demonstrated that the stress for martensitic transformation in NiTi increases significantly with Hf additions. The difference between the stress for slip and the stress for twinning also increases, favoring the latter. This has an important bearing on the reversibility of the transformation, a requirement for the shape-memory effect.

In steels, the martensitic structure undergoes a drastic morphological transition as the carbon content reaches the 0.6–1.0 wt percent region. The current nomenclature is *lath* and *plate*, where the basic difference resides in the deformation mode: slipped (lath) and twinned (plate) martensite. Fig. 2 shows the change in M_s as well as the two modes as a function of increasing carbon content [11]. In Fe–Ni alloys, the same phenomenon takes place.

Here, we review a framework for the quantitative description of the transition from lath to plate martensite and apply it to the Fe–C system. The framework presented here, based on constitutive equations for slip and twinning, can be applied to Fe–Ni–C and thermoelastic martensites, such as in the Ni–Ti system.

The morphologies of lenticular (lath) dislocated and twinned martensites are shown in Fig. 3a for an Fe–30%Ni alloy; Fig. 3b for Fe-22.5 wt%Ni-4 wt% Mn; notice slipped martensite with midrib (Chang and Meyers [12]) and Fig. 3c for a Fe-32 wt%Ni-0.035 wt%C alloy. Notice the formation of twins along the midrib and slip on the outside in Fig. 3c from Thadhani [13] and Thadhani and Meyers [14]. Tamura et al. [15] also observed the different mechanisms of plastic deformation inside the lenses, which he classified into *Shiebung* (for slip) and *Umklapp* (for twinning). His observations consistently indicate, for the same alloy, that the width of the twinned region increases with decreasing temperature.

Fig. 4 shows a schematic representation of slipped, twinned, and mixed martensite.

2. Constitutive description

The calculations require constitutive equations for slip and twinning that have the appropriate temperature and strain rate dependencies. These equations were implemented by Meyers et al. [6] into a slip-twinning transition criterion and will only be briefly described herein by considering slip and twinning as completing mechanisms and equating the appropriate constitutive equations for obtaining the critical condition:

$$\sigma_T = \sigma_S \tag{1}$$

where σ_S and σ_T are the slip and twinning stresses, respectively.

2.1. Constitutive equation for slip

There are numerous equations that successfully incorporate the strain, strain rate, and temperature effects and predict the mechanical response over a broad range of external parameters. Out of many constitutive equations that can be used, including the MTS developed at LANL by Follansbee and Kocks [5], we chose the Zerilli-Armstrong constitutive equation to represent the temperature and strain-rate dependences of the yield stress due to its physical basis and simplicity. The MTS constitutive equation is based on the mechanical threshold stress, which is the extrapolated flow stress at absolute zero temperature (in the absence of thermal activation). Its implementation is more complex.

The Zerilli-Armstrong equation is modified to incorporate the solid solution hardening effects induced by carbon addition. There are three different forms of the Z-A equation applicable to FCC, HCP, and BCC metals. The barrier sizes are quite different: forest dislocations are considered the primary barriers for FCC materials, whereas the Peierls-Nabarro stress is the principal obstacle for BCC materials at low temperatures. The MTS model considers separate shapes of barriers, described by the exponents p and q. It also incorporates the strain-rate dependence of work hardening. This makes the treatment quite complex, and the Z-A constitutive equation presents a more straightforward, but physically correct description.

The BCC structure has a considerably higher strain rate and temperature sensitivities than the FCC structure, which warrants a separate equation. When iron-based alloys undergo the martensitic transformation, the FCC structure transforms to BCC or BCT. This newly created structure has to undergo a complex deformation to accommodate the Bain and lattice invariant strains. The Zerilli-Armstrong equation for the BCC structure has the form:

$$\sigma = C_s \times \exp[T(-C_t + C_r \ln(\dot{\varepsilon}))] + C_h \varepsilon^{C_n} + \sigma_g + \sigma_{cs} \tag{2}$$

The variables are strain, ε, strain rate, $\dot{\varepsilon}$, and temperature, T. The coefficients $C_S, C_t, C_r, C_h, and\ C_n$ are experimentally obtained parameters. They are available in the literature and their physical meanings, and values chosen for pure iron [16] are given in Table 1.

The terms σ_g and σ_{cs} represent the athermal components of stress, which have minimal strain rate and temperature dependence. σ_g rep-

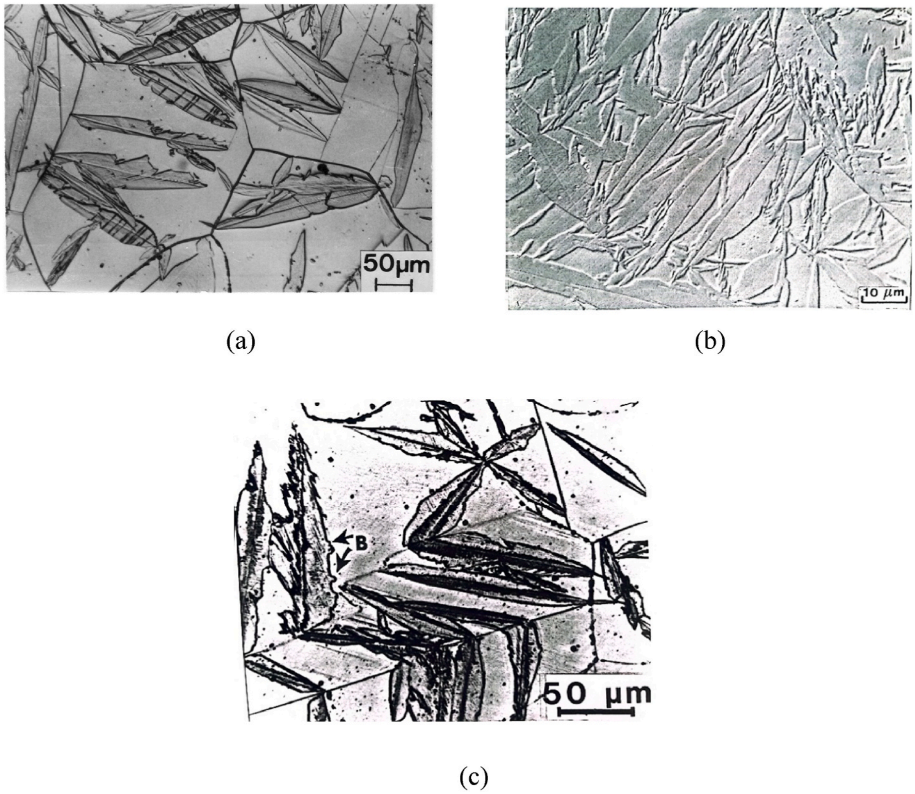

Fig. 3. Slipped, slip-twinned, and twinned martensite lenses; (a) Fe-30 wt% Ni alloy; notice slipped and twinned lenses (courtesy of J. R. C. Guimarães); (b) Fe-22.5 wt%Ni-4 wt%Mn; notice slipped martensite with midrib (Chang and Meyers [12]); (c) Fe-32 wt%Ni-0.035 wt%C Notice the formation of twins along the midrib and slip on the outside (Thadhani and Meyers [14]).

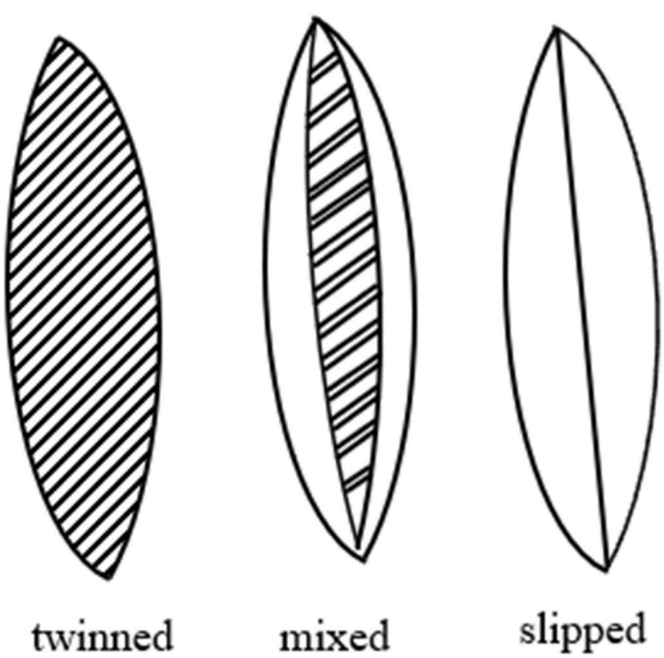

Fig. 4. Schematic representation of three structures of martensite: fully twinned, mixed, and slipped martensite with a midrib; this midrib has been shown to be a thin twinned ribbon by transmission electron microscopy (Tamura et al. [15]; Thadhani and Meyers [14]; Chang and Meyers [12]).

Table 1
Parameters of Zerilli-Armstrong equation.

Z-A Parameter	Symbol	Value
Stress constant	C_s	1033 MPa
Thermal softening exponent	C_t	0.00698
Strain rate constant	C_r	0.000415
Strain hardening constant	C_h	266 MPa
Strain hardening exponent	C_n	0.289

resents the grain-size dependence and is represented by the Hall-Petch relationship:

$$\sigma_g = k_s d^{-1/2} \tag{3}$$

where k_s for low-carbon steels is found to vary between 15 and 18 MPa/mm^{½} [17]. An average value of 16.5 MPa/mm$^{1/2}$ is used in the calculations. The value matches well with experimental data by Marder and Krauss [18]. σ_{cs} represents the contribution to strength due to the presence of solute atoms (in this case, carbon). It is observed that the flow stress at large concentrations of solute varies with the square root of carbon content [19]:

$$\sigma_{cs} = k_{SC}(C_C)^{n_s} \tag{4}$$

n_s is often given as 0.5 and for this case, k_{SC} is 450 MPa. For lower concentrations, Pickering and Gladman [20] use a linear fit to describe the solid solution hardening effect of carbon in austenite with a coefficient of 324 MPa/wt.% carbon. This term was introduced into the ZA equation for BCC metals as separate from the strain term for simplicity. It can be argued that solute hardening increases with strain, but this dependence's form is unknown. Thus, a simple additive term is used here.

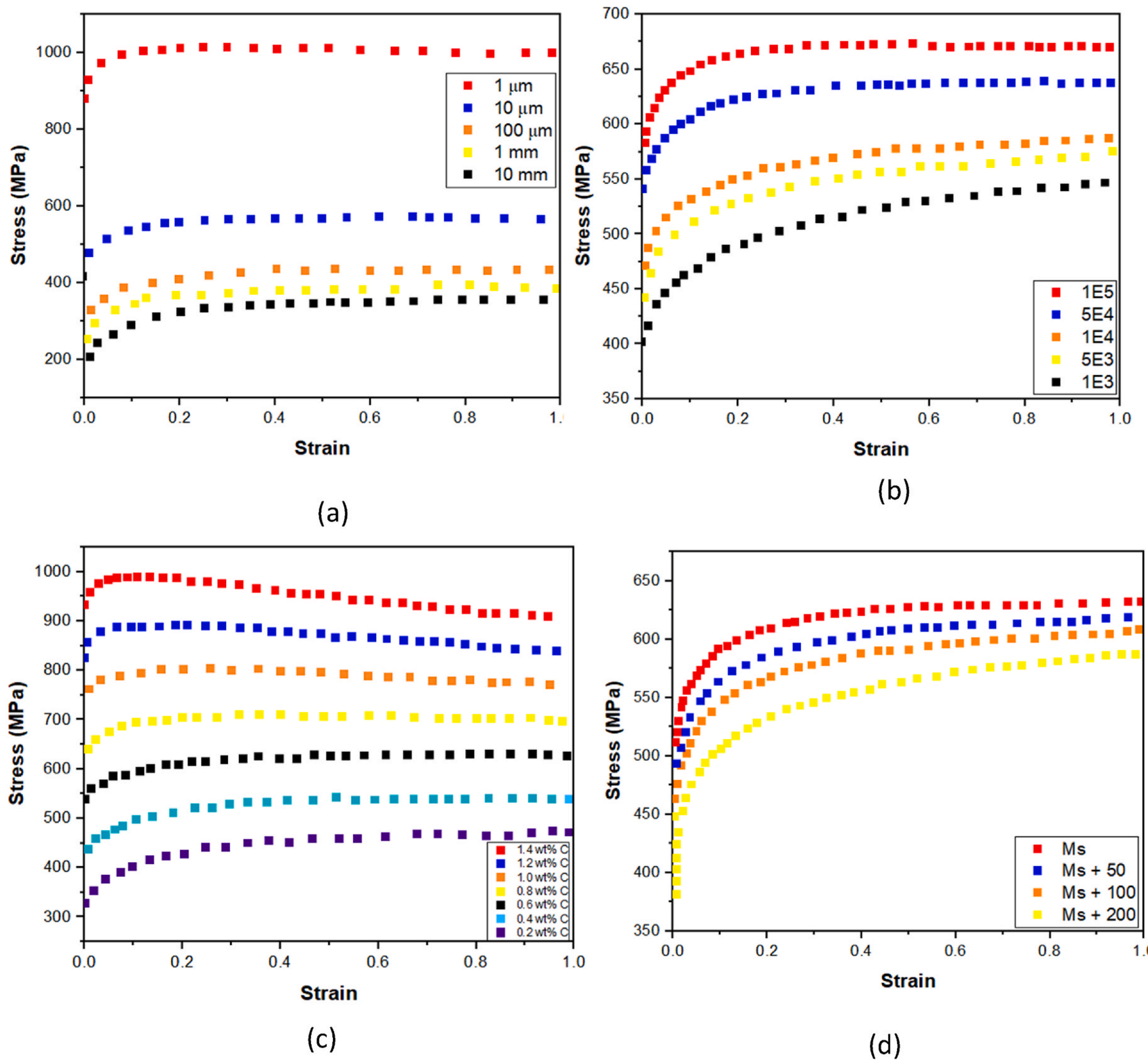

Fig. 5. Calculated stress-strain curves (assuming slip) for different: (a) grain sizes; (b) strain rates; (c) carbon contents (d = 100 μ m; strain rate = 10^4 s^{-1}); (d) temperatures above M_S.

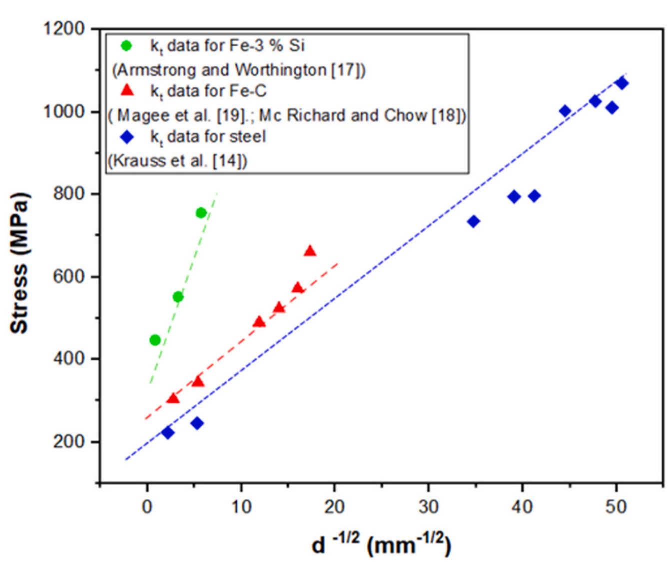

Fig. 6. Effect of grain size, d, on the twinning stress for steel, Fe–C, and Fe–Si alloys.

Fig. 5 shows the predicted stress-strain curves for different (a) grain sizes; (b) carbon contents; (c) strain rates; and (d) temperatures.

2.2. Constitutive equation for twinning

In the current calculations, the twinning stress is assumed to be relatively independent of strain, temperature, and strain rate, in contrast to slip processes. Therefore, no work-hardening effects are taken into account. Nevertheless, the grain-size dependence is much larger than for slip. Indeed, k_T values are 2–4 times greater than k_S values. Fig. 6 shows the Hall-Petch plots for twinning. The following equation is used, to which the strengthening effect due to solid solution is incorporated:

$$\sigma_T = \sigma_O + \sigma_{cT} + k_T \, d^{-1/2} \tag{5}$$

Armstrong and Worthington [21] report for Fe–3%Si: k_T = 66.3 MPa/mm$^{1/2}$. For low-carbon iron, McRickard and Chow [22] and Magee et al. [23] report values of 45.5 MPa/mm$^{1/2}$. This latter value is used here. The strengthening effect due to solute carbon atoms, also has to be inserted into Eqn. (5). Fig. 7 shows experimental results by Magee et al. [23] for Fe-4.8 at% Sn-X% C, where the carbon content varies from 0.019 to 0.089 at% C. Magee et al. [19] used a linear fit expressed as:

$$\sigma_{cT} = 368 + 1040 at\%C \tag{6}$$

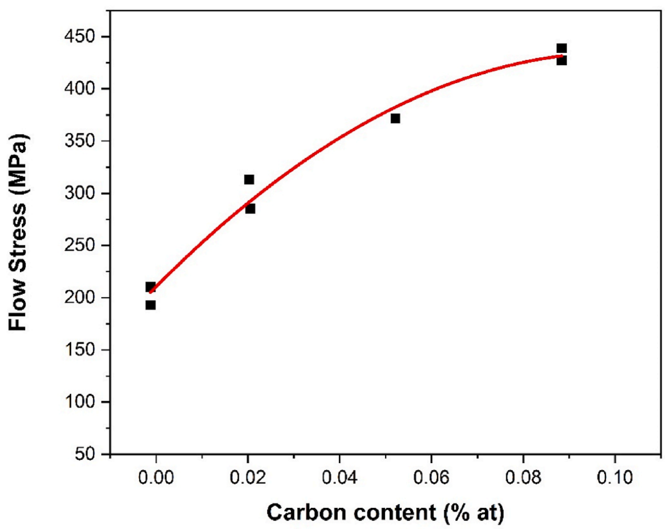

Fig. 7. Effect of interstitial carbon on the compressive flow stress of iron-carbon alloys (Fe-4.8 at% Sn-x% C, where the carbon content varies from 0.019 to 0.089 at%C) deformed by twinning; the data for the carbonless alloy is taken (Adapted from Magee et al. [23]).

This was replaced in the present calculations by a power fit:

$$\sigma_{cT} = k_{TC}(C_C)^{n_T} \tag{7}$$

where k_{TC} is equal to 662 MPa and n_T is equal to 0.158. The linear equation which agrees with the theories of Cottrell [24] and Bilby [25]. This equation has the form:

$$\sigma(\text{MPa}) = 368 + 1040 \text{ at\% C} \tag{8}$$

However, we kept the power expression in order to retain the same calculations.

The twinning stresses are extrapolated from Fig. 6 for higher concentrations of carbon. Fig. 7 shows the predicted stress-strain curves for different (a) grain size and (b) carbon contents.

2.3. Martensitic strains and strain rates

Fig. 8b shows, in a schematic fashion, the growth of the martensite lens. The material within the expanding lens is subjected to Bain and lattice invariant strains in Fig. 8 a. There is an undistorted and unrotated plane, which is indicated by a red line. It is known as the habit plane. There are essentially two crystallographic relations and orientations of the habit plane of lenticular martensite: Depending on the crystallography, Kurdjumov-Sachs [26] or Nishiyama-Wasserman [27] orientations are observed, with habit planes of (225) and (259), respectively. It is assumed, for the Fe–Ni and Fe–C alloys, that the nucleation is classic and follows the Olson-Cohen [28] mechanism. So, no lattice softening, that would change the morphology during the early stages of growth, is considered.

During martensitic transformation, the strain rate can be approximated by:

$$\dot{\gamma} = \frac{\gamma}{t} \approx \frac{\gamma \nu}{D} \tag{7}$$

where ν is the growth velocity for the martensite lens, γ is the transformation strain ($\gamma = 0.2$)`and D is the grain diameter. In Fig. 8b, two growth directions are indicated: longitudinal and transverse growth.

Meyers [29] has analyzed the two modes and discusses the two

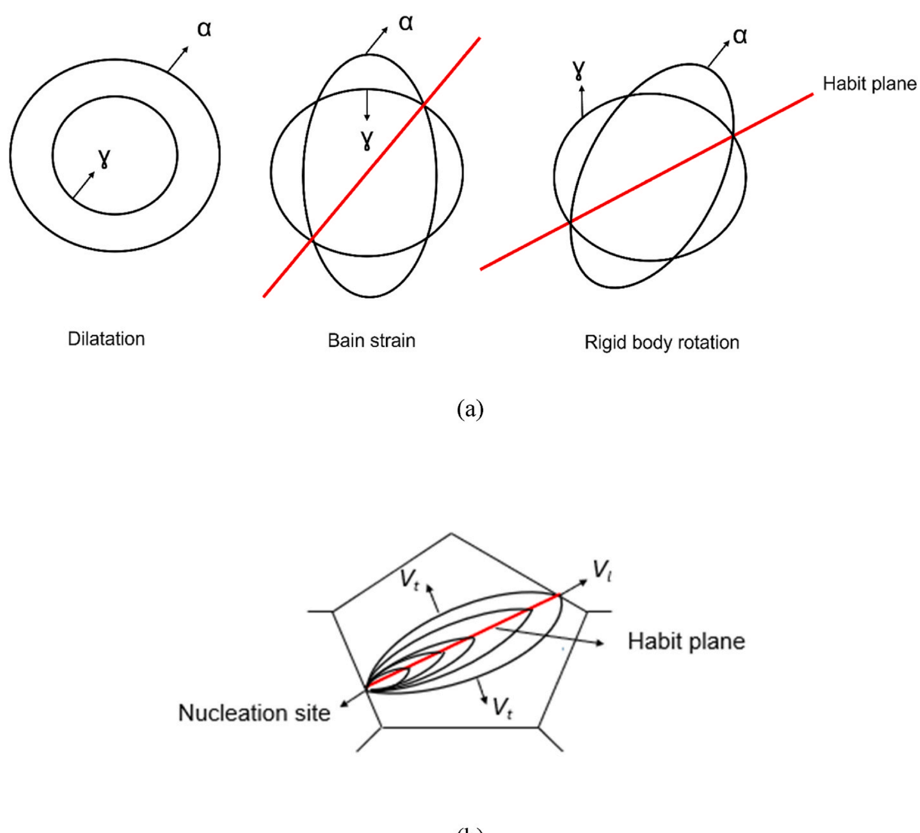

Fig. 8. (a) Three components of martensitic transformation: dilatation in transformation; transformation of sphere into ellipsoid; rotation. (b) Schematic representation of growth of martensite lens with longitudinal (V_l) and transverse (V_t) growth velocities. Notice that the midrib corresponds to habit plane in (a).

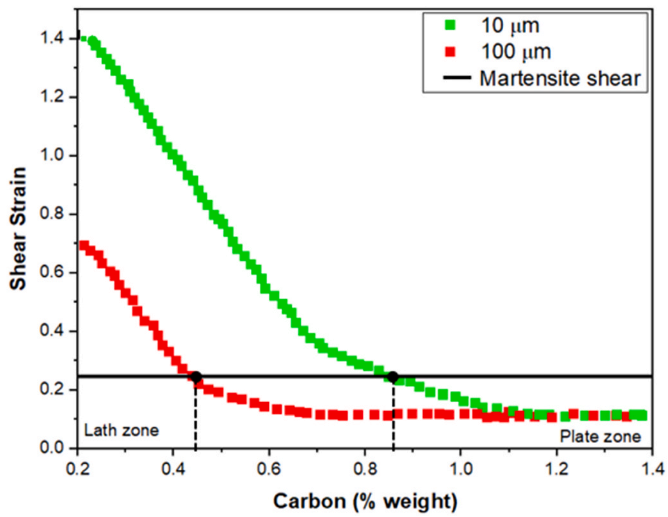

Fig. 9. Predicted shear strain at which slip to twinning transition occurs as a function of carbon content for two sizes of grains; the shear strain for martensitic transformation is assumed to be equal to 0.26 (horizontal line in the plot). The intersection marks the carbon content at which the transition occurs. For a grain size of 100 μm, it is ~0.43 wt % C and for 10 μm it is ~0.84 wt % C (intersections circled).

velocities. The longitudinal growth velocity has been measured by Bunshah and Mehl [30] for Fe–Ni–C alloys; it was found to be equal to 1000 m/s. Schoen and Owen [31] measured the lateral growth velocity for Fe–10%Ni–C alloys with carbon contents between 0 and 0.010. the values varied from 0.01 to 1 m/s. Considering a range of velocities of 1–1000 m/s, one obtains a range of strain rates:

$$\dot{\gamma} = \frac{0.20 \times \nu}{D} \approx \frac{1}{D}\ (0.2 \rightarrow 200) \tag{8}$$

For a grain size of 100 μm (a reasonable value for Fe alloys), one obtains the following range of strain rates: $\dot{\gamma} = 2\text{x}10^3 \rightarrow\ 2\text{x}10^6\ \text{s}^{-1}$

In the calculations conducted and reported herein, a strain rate of $10^3\ \text{s}^{-1}$ was assumed. It is interesting to notice that the strain rate along the mid-rib (region subjected to longitudinal growth) is much higher. It is also observed that this region is more prone to twinning. Often, one observes martensite lenses with twinning along the mid-rib and dislocations in the lateral growth regions.

The slip-twinning transition has to be determined at the shear strain inside the martensite lens. The flow stress by slip increases with strain, whereas the twinning stress is assumed to be constant. Calculations were conducted for two-grain sizes: 10 and 100 μ m. The results of the computations are shown in Fig. 9. The curves indicate the shear strains at which the slip nd twinning stresses are equal as a function of carbon content. Since the shear strain required by the transformation is equal to 0.256, martensite is slipped if this strain at equality is above this value. Conversely, if the shear strain is smaller than 0.256, twinning is favored. For the 100 μ m grain size, the predicted transition from dislocated to twinned martensite is in good agreement with the observed results: 0.43 wt% C. As the grain size decreases, the transition carbon content increases to 0.84 wt% C.

3. Conclusions

- The slip-twinning transition criterion postulated by Thomas [8,9] and quantified by Meyers et al. [7] is applied to the martensitic transformation. This constitutive description applies to the change in morphology from lath to plate and within the plates themselves and is therefore of a general nature.
- It is based on the assumption that slip and twinning are competing plastic deformation mechanisms and that the one requiring least stress under the imposed conditions of temperature, strain rate, and internal parameters dictates the nature of the process during the transformation.
- The constitutive response by slip is described here by the Zerilli-Armstrong equation with the addition of grain size and interstitial strengthening terms. A simple non-work hardening twinning equation, also incorporating grain size and carbon concentration terms, is used. The slip-twinning transition is obtained by making $\sigma_s = \sigma_t$
- The model predicts change from lath (slipped) to plate (slip and/or twinned) martensite in the Fe–C system as carbon content exceeds 0.43 wt%, at a grain size of 100 μm. This agrees with the experiments. It is interesting to notice that the predicted change in lath-to-plate morphology is dependent on the austenitic grain size.
- This constitutive competition between two deformation mechanisms can be applied to the Fe–Ni–C and thermoelastic Ni–Ti systems and can predict the regimes of reversibility, since slip is essentially irreversible whereas twinning can be reversed through the motion of glissile interfaces. Many important parameters, such as strain rate and strain state, affect the kinetics of martensitic transformation and its morphology, but they can be rationalized in terms of the proposed constitutive model (Murr et al. [32]; Staudhammer et al. [33]).

Declaration of competing interest

The authors declare that they have no known competing financial interests or personal relationships that could have appeared to influence the work reported in this paper.

Acknowledgments

We thank Dr. M. S. Schneider for making the plots and for numerous enlightening discussions. We dedicate this contribution to the memory of Prof. U. F. Kocks, who brought life and energy to the UCSD Materials and Mechanics seminars for ten years. Prof. J. R. C. Guimaraes kindly sent us Fig. 3a. Fig. 3b and c were extracted from the dissertations of N. N. Thadhani and S. N. Chang with their permission. We thank the Center for Matter Under Extreme Conditions (CMEC) for support under Department of Energy- National Nuclear Security Administration Grant No. DE-NA0004147.

References

[1] Ashby MF. Models for plastic flow: people, places, concepts and techniques. J Mater Res Technol 2024:1–7.
[2] Kocks UF. A statistical theory of flow stress and work-hardening. Philos Mag A J Theor Exp Appl Phys 1966;13:541–66. https://doi.org/10.1080/14786436608212647.
[3] Kocks UF, Argon AS, Ashby MF. Thermodynamics and kinetics of slip. Prog Mater Sci 1975;19:291.
[4] Mecking H, Kocks UF. Kinetics of flow and strain-hardening. Acta Metall 1981;29:1865–75.
[5] Follansbee PS, Kocks UF. A constitutive description of the deformation of copper based on the use of the mechanical threshold stress as an internal state variable. Acta Metall 1988;36:81–93. https://doi.org/10.1016/0001-6160(88)90030-2.
[6] Lu CH, Remington BA, Maddox BR, Kad B, Park HS, Prisbrey ST, et al. Laser compression of monocrystalline tantalum. Acta Mater 2012;60:6601–20. https://doi.org/10.1016/j.actamat.2012.08.026.
[7] Meyers MA, Vöhringer O, Lubarda VA. The onset of twinning in metals: a constitutive description. Acta Mater 2001;49:4025–39. https://doi.org/10.1016/S1359-6454(01)00300-7.
[8] Johari O, Thomas G. Factors determining twinning in martensite. Acta Metall 1965;13:1211–2. https://doi.org/10.1016/0001-6160(65)90060-X.
[9] Thomas G. Electron microscopy investigations of ferrous martensites. Metall Trans A 1971;2:2373–85.
[10] Wang J, Sehitoglu H. Modelling of martensite slip and twinning in NiTiHf shape memory alloys. Philos Mag A 2014;94:2297–317. https://doi.org/10.1080/14786435.2014.913109.
[11] Krauss G. Principles of heat treatment of steel. Metals Park: OH: ASM; 1980. p. 52.
[12] Chang S-N, Meyers MA. Martensitic transformation induced by a tensile stress pulse in Fe-22.5 wt% Ni-4wt% Mn alloy. Acta Metall 1988;36:1085–98.
[13] Thadhani NN. An investigation into martensitic transformation induced by a tensile stress pulse. New Mexico Institute of Mining and Technology; 1984.

[14] Thadhani NN, Meyers MA. Kinetics of martensitic transformation induced by a tensile stress pulse. Acta Metall 1986;34:1625–41. https://doi.org/10.1016/0001-6160(86)90109-4.
[15] Tamura I, Maki T, Hato H. On the morphology of strain-induced martensite and the transformation-induced plasticity in Fe-Ni and Fe-Cr-Ni alloys. Trans Iron Steel Inst Japan 1970;10:163–72. https://doi.org/10.2355/isijinternational1966.10.163.
[16] Armstrong RW, Zerilli FJ. Dislocation mechanics aspects of plastic instability and shear banding. Mech Mater 1994;17:319–27.
[17] Pickering FB. Constitution and properties of steels, vol. 7. VCH; 1992.
[18] Marder A, Krauss G. Proc. On the strength of metals and alloys, vol. 3. Metals Park: OH: ASM; 1970.
[19] Pickering FB. Physical metallurgy and the design of steels. Essex, England: Applied Science Publishers; 1978.
[20] Pickering FB, Gladman T. Metallurgical developments in carbon steels. ISI Spec Rep 1963;81.
[21] Armstrong R, Worthington P. In: Rohde RW, Bitcher BM, Holland JR, Karnes C, editors. Metallurgical effects at high strain rates. New York: Plenum Pre; 1974. p. 401–14.
[22] McRickard S, Chow JG. No title. Trans AIME 1965;223:147.
[23] Magee CL, Hoffman DW, Davies RG. The effect of interstitial solutes on the twinning stress of bcc metals. Philos Mag A J Theor Exp Appl Phys 1971;23:1531–40.
[24] Cottrell AH. Report of a conference on strength of solids, vol. 30; 1948.
[25] Bilby BA. On the interactions of dislocations and solute atoms. Proc Phys Soc 1950;63:191.
[26] Kurdjumow G, Sachs G. Über den mechanismus der stahlhärtung. Zeitschrift Für Phys 1930;64:325–43.
[27] Nishiyama Z. No title. Sci Rep Tohoku Univ 1934;28.
[28] Olson GB, Cohen M. A general mechanism of martensitic nucleation: Part II. FCC→BCC and other martensitic transformations. Metall Trans A 1976;7:1905–14.
[29] Meyers MA. On the growth of lenticular martensite. Acta Metall 1980;28:757–70. https://doi.org/10.1016/0001-6160(80)90153-4.
[30] Bunshah RF, Mehl RF. The rate of propagation of martensite. Trans. AIME 1953;197:1251–8.
[31] Schoen FJ, Owen WS. Interfacial drag and the growth of martensite. Metall Trans A 1971;2:2431–42. https://doi.org/10.1007/BF02814880.
[32] Murr LE, Staudhammer KP, Hecker SS. Effects of strain state and strain rate on deformation-induced transformation in 304 stainless steel: Part II. Microstructural study. Metall Trans A 1982;13:627–35.
[33] Staudhammer KP, Murr LE, Hecker SS. Nucleation and evolution of strain-induced martensitic (bcc) embryos and substructure in stainless steel: a transmission electron microscope study. Acta Metall 1983;31:267–74.